Registration of Liver Images to Minimally Invasive Intraoperative Surface and Subsurface data

Yifei Wu[a], D. Caleb Rucker[b], Rebekah H. Conley[a], Thomas S. Pheiffer[a], Amber L. Simpson[a], Sunil K. Geevarghese[c], Michael I. Miga[a],

[a]Vanderbilt University, Dept. of Biomedical Engineering, Nashville TN;
[b]University of Tennessee-Knoxville, Dept. of Mechanical Engineering, Nashville TN;
[c]Vanderbilt University Medical Center, Nashville TN

ABSTRACT

Laparoscopic liver resection is increasingly being performed with results comparable to open cases while incurring less trauma and reducing recovery time. The tradeoff is increased difficulty due to limited visibility and restricted freedom of movement. Image-guided surgical navigation systems have the potential to help localize anatomical features to improve procedural safety and achieve better surgical resection outcome. Previous research has demonstrated that intraoperative surface data can be used to drive a finite element tissue mechanics organ model such that high resolution preoperative scans are registered and visualized in the context of the current surgical pose. In this paper we present an investigation of using sparse data as imposed by laparoscopic limitations to drive a registration model. Non-contact laparoscopically-acquired surface swabbing and mock-ultrasound subsurface data were used within the context of a nonrigid registration methodology to align mock deformed intraoperative surface data to the corresponding preoperative liver model as derived from pre-operative image segmentations. The mock testing setup to validate the potential of this approach used a tissue-mimicking liver phantom with a realistic abdomen-port patient configuration. Experimental results demonstrates a range of target registration errors (TRE) on the order of 5mm were achieving using only surface swab data, while use of only subsurface data yielded errors on the order of 6mm. Registrations using a combination of both datasets achieved TRE on the order of 2.5mm and represent a sizeable improvement over either dataset alone.

Keywords: image guided surgery, liver, deformation, conoscope, subsurface, nonrigid, registration

1. INTRODUCTION

Before an operation, a surgeon usually has preoperative imaging data to allow visualization and localization of the tumor and anatomical landmarks. X-Ray Computed Tomography (CT) and Magnetic Resonance Imaging (MRI) are commonly employed due to their high spatial resolution and contrast. The images are helpful for surgical planning but are often underutilized during a surgery because of the substantive difference in presentation between the preoperative and intraoperative states. In addition, organs shift and non-rigid deformations occur due to mobilization where connective tissue is resected to mobilize the liver and padding is added to stabilize the presentation of resection entry surfaces.[1]

In contrast to preoperative imaging modalities, intraoperative imaging is usually more expensive and potentially cumbersome due to workflow limitations resulting in interference with other surgical equipment. Alternatively, one could use model-based registration methods to align preoperative image information to the intraoperative setting. Registration usually uses sparsely acquired intraoperative patient localization data (e.g. optically-tracked stylus surface swabs or tracked intraoperative ultrasound) to transform the preoperative scan images into the pose as seen in the operating room (OR). A good registration can help the surgeon to define tumor margins and improve surgical outcomes.

Prior studies have examined the feasibility of using sparse surface data for liver registration. Clements[2] proposed using tracked surface swabs of salient anatomical features for use in a robust rigid registration that rotates the preoperative images to match the intraoperative orientation. Subsequent work from Dumpuri[3] and Rucker[4] investigated using a linear elastic finite element model created from the preoperative patient CT to calculate a displacement field that describes the organ deformation. For these studies, the data is assumed to come from open surgery cases where a laparotomy or similar incisions allow relatively large extents of the liver surface to be visible. Intuitively, the registration accuracy decreased as visibility is reduced, but it is not known whether a useful registration can be obtained with small extents as might be found in minimally invasive cases. In addition to reduced recovery time and trauma, studies suggest that the short and long term outcomes of laparoscopic liver resection (LLR) are comparable to those of open surgery[5]. However, compared to open surgery, LLR poses additional challenges to surgeons to achieve the same oncological standards. Some problems include reduced field of view, reduced depth of field and inability to palpate tissue. These factors increase the difficulty of following surgical resection plans that ensure negative tumor margins and preserve liver volume and function.

The limitations in visibility increase the value of a surgical navigation system that could accurately track and display registered images during surgery, especially in the presence of nonrigid deformations. However, these surgical limitations also affect the extent and quality of registration data that can be collected. Ultrasound features are commonly collected in minimally invasive cases and can potentially be used to guide registrations. The goal of this work is to investigate a method of obtaining intraoperative data in a LLR context and to compare the feasibility of image-to-physical registration as compared to that in the open environment. In short, we would like to compare the accuracy of a registration based on LLR data against the "bronze standard" of what is obtainable in an open case.

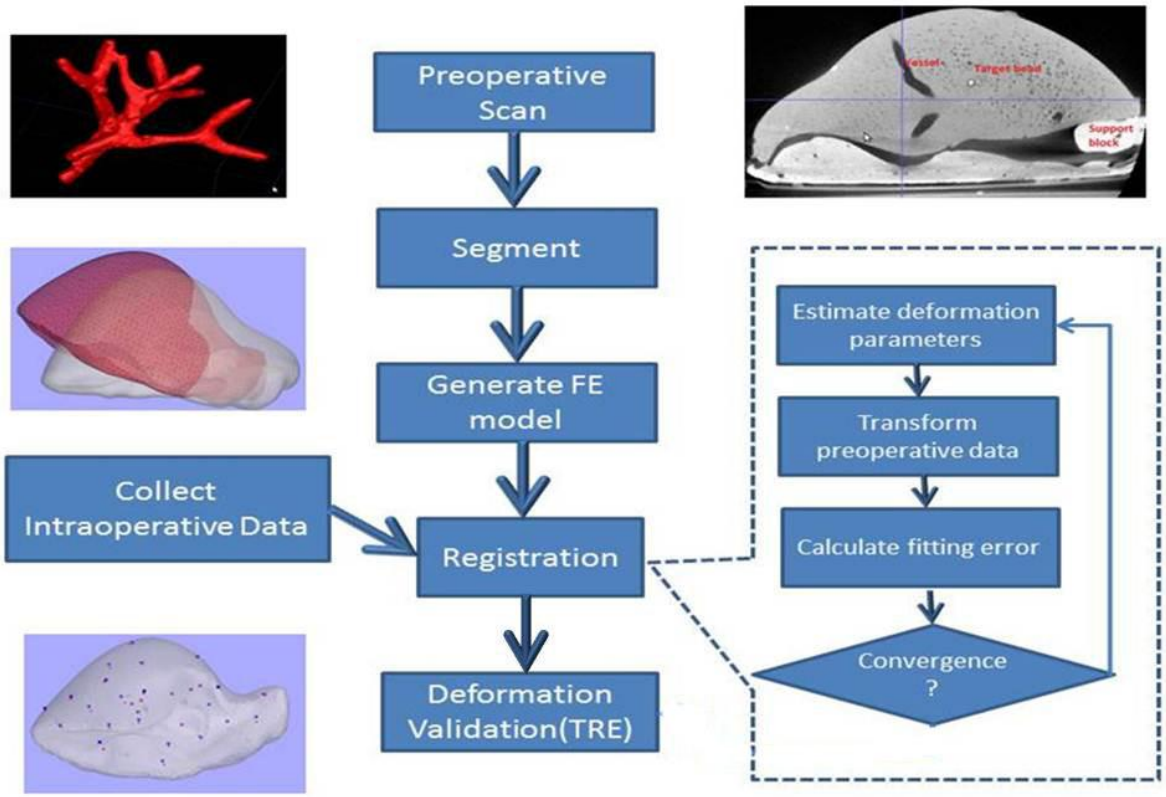

Figure 1: General overview of our registration workflow (dashed box is a call-out covering the iterative steps of the optimization algorithm).

Further author information: (Send correspondence to Michael I. Miga)

E-mail: Michael.I.Miga@vanderbilt.edu, Telephone: 1-615-343-8336, Web: http://bmlweb.vuse.vanderbilt.edu

2. METHODS

There are 3 major steps involved for accurate image-to-physical alignment and navigation. 1) A preoperative scan of the relevant organ is segmented and digitized into a soft tissue biomechanical Finite Element (FE) model, 2) a set of intraoperative data is collected and finally, 3) the registration algorithm is used to calculate the displacement field describing how the preoperative model should be deformed to match the intraoperative data. The registration framework used is based on the work of Rucker[4]. Figure 1 shows an overview of the registration process and the steps are described in more detail below.

2.1 Segmentation and generation of a patient specific preoperative model

The liver is imaged by CT to obtain a raw tomogram. The image slices are manually segmented to obtain a clean representation of the geometry of the organ. The segmented images are converted to a 3D volume using the Marching Cubes algorithm[6]. The volume is filtered using radial basis functions to reduce surface noise. A custom-built mesh generator algorithm based on Sullivan[7] is used to create the tetrahedral elements for the 3D finite element models.

2.2 Intraoperative data acquisition

Information about the deformed intraoperative state is captured to drive the registration. Surface and subsurface data are collected from the deformed intraoperative state of the mock organ. The surface topography is acquired as a digitized point cloud representation using tracked surface swabs. There are 3 common methods of surface digitization – manual stylus contact swabbing, conoscopic holography, and laser range scanning. The manual stylus suffers from contact error as the swabs are being performed i.e. the operator presses on the surface and deforms the tissue. The LRS is not suitable for minimally invasive cases due to its size. We used the conoscope for our phantom experiments because there is no contact error and the optical data can be collected through a laparoscopic port. The feasibility of using this device has been investigated previously[8] with encouraging results. The subsurface information can be acquired through tracked intraoperative ultrasound. In this work, we used CT data to simulate the reconstruction of 3D subsurface vessels derived from tracked ultrasound scanning.

2.4 Registration algorithm

Anatomical features are designated on the preoperative images and corresponding landmarks are obtained from the intraoperative state. An initial rigid alignment between the model and the intraoperative data is made by using the weighted salient anatomical feature algorithm previously described by Clements[2]. With respect to visible features often present during open liver surgery, the falciform ligament, round ligament, and inferior ridges are often available as salient features. It should be noted that not all salient features are needed to achieve a good alignment.

A Priori, we assume that the majority of deformation is induced by changes in the support surface on the posterior of the liver. The liver is often propped up by surgical towels for presentation in open cases, and by laparoscopy pads in LLR cases. Thus the assumed main modes of deformation are induced by a change in the posterior surface. To simplify the parameterization of posterior boundary conditions, a loading function was defined by a bivariate 3rd degree polynomial that prescribed nodal displacements in the direction of the mean normal direction of the posterior surface (Equation 1).

$$u = \hat{\boldsymbol{n}} \sum_{1 \le i+j \le n}^{n} c_{ij} t_1^i t_2^j \qquad (1)$$

$\boldsymbol{u}$ represents the nodal displacement vector,
$\hat{\boldsymbol{n}}$ represents the unit vector of the mean normal direction of the posterior surface,
$\boldsymbol{t_1}$ and $\boldsymbol{t_2}$ represent the tangential coordinates of the node,
$\boldsymbol{c}$ represents the polynomial coefficients
$\boldsymbol{n}$ is the highest polynomial degree of the displacement field..
$\boldsymbol{i}$ and $\boldsymbol{j}$ represent exponents. The summation is used to exclude redundant rigid rotational modes.

The surface nodes on the liver posterior were defined to have these loading conditions while other nodes were defined to be stress free.

The registration algorithm minimizes an objective function that describes the misfit between the preoperative model surface and the intraoperative surface/subsurface points. Correspondence is assigned by closest point correspondence--intraoperative and preoperative points of the current estimated deformation are assumed to correspond if they are the closest neighbors. When available, subsurface points are used in a similar manner to the surface points. The objective function is calculated as follows:

$$G(\Psi) = \frac{1}{N}\sum_{i=1}^{N}\left(\hat{n}_{ci}^{T}(p_{di} - p_{ci})\right)^2 + \alpha_1 U^2 + \sum_{j=1}^{M}\alpha_2 \left\|p_{dj} - p_{cj}\right\|^2 \quad (2)$$

$$U = u^T K u \quad (3)$$

$$\Psi = \{\bar{c}, t_x, t_y, t_z, \theta_x, \theta_y, \theta_z\} \quad (4)$$

N is the number of surface points collected intraoperatively
M is the number of subsurface intraoperative points
$\hat{n}_{ci}$ is the unit normal vector to the model surface at point pci
p_{di} are the coordinates of the surface point cloud
p_{ci} are the coordinates of the corresponding model surface node
α_1 is a smoothness constraint scaling constant
U is the total energy stored in the nonrigid displacement field and is defined by equation 3 where u and K represent the displacement vector and the stiffness matrix respectively
α_2 is a scaling constant to adjust the relative strength of the contribution of the subsurface points to the solution
p_{sj} is the coordinates of the subsurface point cloud
p_{dj} is the coordinates of the corresponding model subsurface node

The coefficients of the posterior displacement polynomial, the translations associated with rigid spatial alignment and the angles associated with rigid rotation, constitute the optimization parameter set, Ψ, as defined in equation 4. We then use the Levenberg-Marquardt algorithm to find the best nonrigid and rigid parameters that transforms the model to fit the intraoperative data.

2.5 Phantom Experiments

A set of phantom experiments were performed to simulate data that can be collected in an LLR case. An abdomen laparoscopy trainer box (Karl Storz, Germany) was used to constrain and simulate the physical limitations of laparoscopic ports (see Fig. 2, 3). The phantom had 8 access ports to allow laparoscopic tools access to the cavity. Three were used in the experiment as indicated in Fig. 3 right.

The phantom was made similar to the one described in Rucker[4]. Briefly, an Ecoflex(Smooth-On, PA) silicone phantom in the shape of a human liver was cast with embedded surface and subsurface targets. A total of 29 CT-opaque target beads were implanted to track the displacement of the liver to validate the calculated displacement field from the nonrigid registration methodology above. In addition, blood vessels were simulated by inserting wax vessel molds into the portal triad area. After casting, the wax was removed by heating and melting commonly known as lost-wax casting. The diameter sizes of the vessels are on the order of larger vessels found in human livers[9].

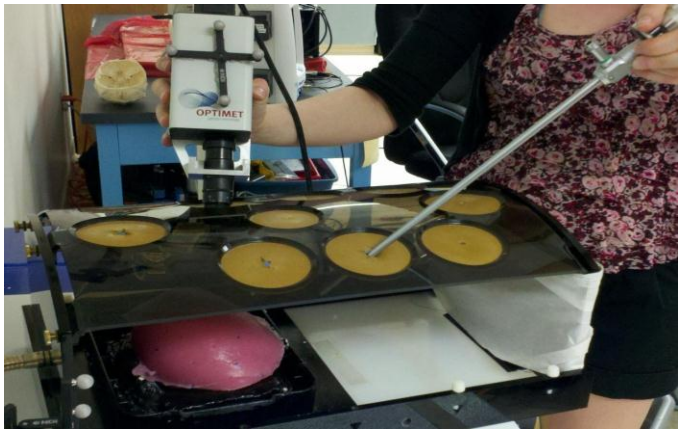

Figure 2: Experimental Setup

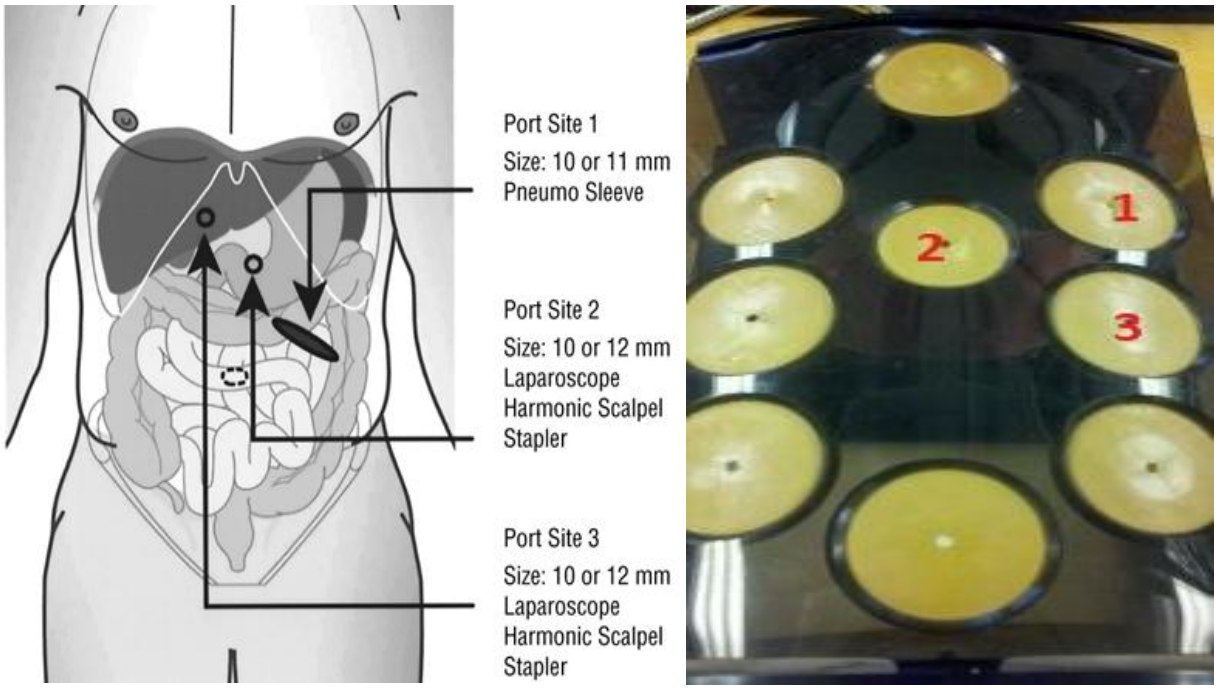

Figure 3: Left: Port locations from Fong[10]. Right: Port designations for experiment

2.6 Conoscopic measurements

An Optimet Mark 10 conoscope (Jerusalem, Israel) was used to digitize the phantom surface into a point cloud. The conoscope was mounted on a custom-built bracket with passive optical markers fixed on a rigid body. A NDI Polaris (Waterloo, Canada) camera was used to track the position of the rigid body. The data collection system was calibrated to map the distance offset of the conoscope into a 3D point coordinate[11]. In a previous study, the accuracy of conoscope swabbed data at realistic laparoscopic distances was found to be similar or superior to LRS[8].

2.7 Phantom Data Collection

With respect to protocol, prior to intraoperative collection, a reference "mock preoperative" CT scan was taken. This represents the state of the undeformed organ before surgical presentation. Then, intraoperative deformations were simulated by adding solid supports underneath the mock organ to change the support surface on the posterior organ surface (Fig. 4). For each deformed pose, surface data was recorded through three different ports using the conoscope as a non-contact swabbing digitizer. After collection, a CT of the deformed state was taken to establish the true location of all surface and subsurface target beads and to obtain the true deformed surface geometry. Subsurface and large surface extent data was retrospectively obtained from segmenting the deformed state CT. A total of 3 different poses were induced to represent variations in clinical presentation.

Laser Range Scanner data was simulated by using the segmented CT volume. A patch of surface points with extent similar to what is observed in clinical cases was extracted and down-sampled to reduce computational time in registration. Subsurface data was obtained by segmenting the CT volume for the blood vessels and vessel boundaries were obtained by using the snake algorithm and manually initialized seeds designated at the vessel centerlines.

2.8 Target Registration Error Calculations

The accuracy of our model was evaluated by use of the target beads implanted into the phantom. The preoperative scan was used to establish the starting positions of the beads and an intraoperative CT was taken after each of the deformations. After registration, the intraoperative bead locations are compared to their registered preoperative counterparts. To calculate the mean target error, the Euclidean distances between the registered and true positions are calculated and we report the root mean square of the target error vector (TRE).

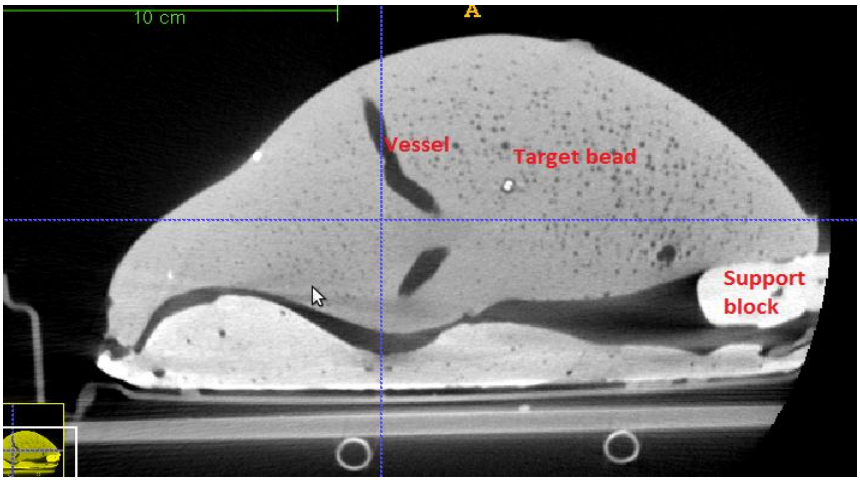

Figure 4: CT of phantom with support blocks, 'blood' vessels and target beads

3. RESULTS

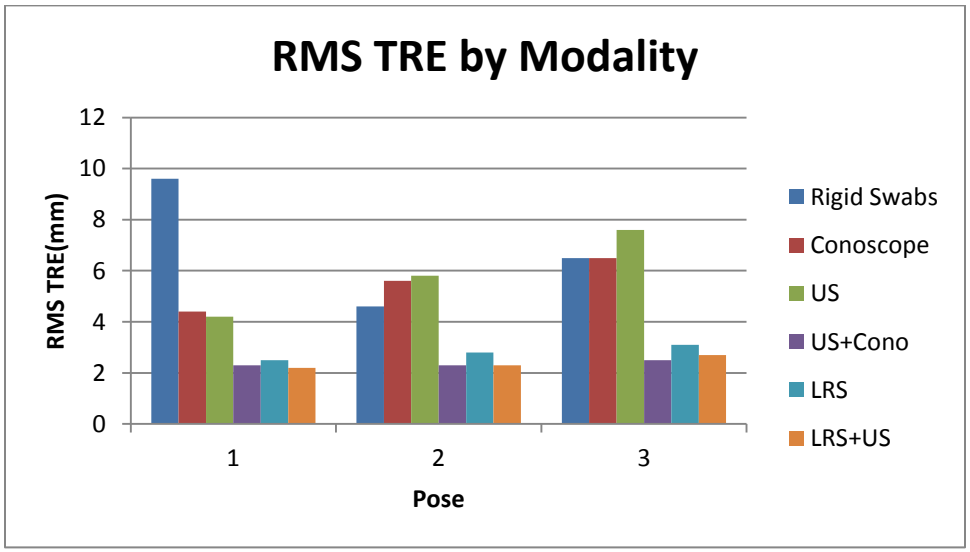

Figure 5: Effects of Different Modalities. This figure compares the accuracy of using different amounts/types of data in the nonrigid registration. 'Cono' represents the registration using the conoscope surface data. 'US' uses only subsurface vessel wall points. 'US+cono' uses both surface and subsurface points. 'LRS' uses a large extent surface patch and 'LRS+US' uses both the large surface patch data and subsurface information. Rigid results are provided as a baseline starting point for all nonrigid steps.

Figure 5 compares the registration results of using various surface data and when subsurface data was used in conjuction with the surface data. 'Rigid swabs' represents results after a rigid alignment using conoscope swabbed salient features. This initialization serves as a baseline starting point for all subsequent nonrigid registration. Registrations using only conoscope surface swabs and the registrations using only subsurface data had accuracy similar to those obtained from a rigid registration. When subsurface and surface information was used together (Cono+US), the results were improved and similar to registrations using large surface coverage (LRS). Using subsurface information with the large surface extent data to register (LRS+US) did not seem to add further improvement as compared to just using LRS.

The results were visualized to assess the quality of the registrations. Figure 6 shows the result of nonrigid registrations using both conoscope and subsurface data. We note that the predicted bead locations look aligned with the true bead locations and there were no unaccounted for or unmatched beads (Figure 6 top-left). There is a marked improvement of

predicted bead locations from the nonrigid registration over the rigid alone. Figure 6 right depicts the registration of the deformed vessel wall to the intraoperative data. The registration performance seems reasonable since most of the deformed points match up to the vessel walls. It is also worth noting that the nonrigid registration preserved the general structure of the vessels—the shape is similar to the preoperative state but the vessels are deformed to conform to the intraoperative data.

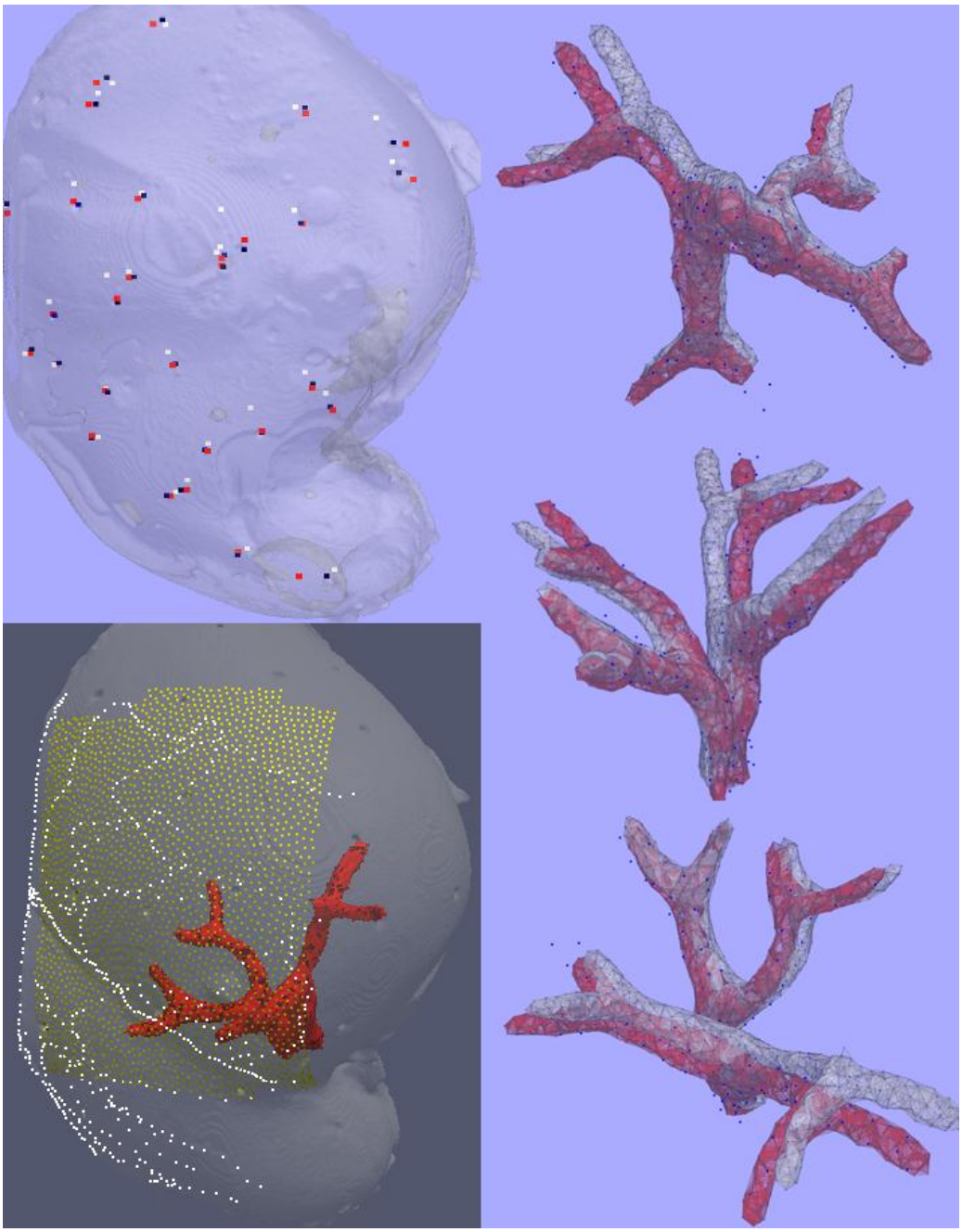

Figure 6 Top-Left: Bead locations after registration--blue represents the true intraoperative locations and red represents the model predicted locations, white represents rigid registration results. Right: Vessels before and after registration. The blue represents the true intraoperative vessel wall after downsampling to simulate US sparsity. The red represents the nonrigidly registered preoperative vessel. The white represents the preoperative vessel rigidly registered. Bottom-Right: Spatial extents and density of the data sets used. White represents the conoscope feature and surface swabs, yellow shows the LRS surface cloud and red represents the preoperative vessels.

4. CONCLUSIONS

We have simulated the collection of surface and subsurface data from a minimally invasive case and proposed a method of using this mock intraoperative data to register a preoperative liver volume. In our phantom experiments we showed that the use of both surface and subsurface data produces higher accuracies than use of either set alone We conclude that the proposed registration algorithm is feasible and can be used to accurately predict displacements within the organ.. Future work will attempt to quantify the extent data quantity and quality influence registration accuracy.

ACKNOWLEDGMENTS: This work is funded by the National Institutes of Health, under the National Cancer Institute Grant No. R01CA162477. We thank Mike Delisi and Dr Galloway for their generous contribution of laparoscopic equipment, Ray Lathrop for developing the conoscopic mounting bracket used in this study and Amber Simpson for coding the conoscope module. We are also thankful for Ramya Balachandran, Wendy Lipscomb, and Dr Labadie for their crucial role in allowing me to get CT of the phantoms, and Jordan Halasz at CELA for supplying the abdominal laparoscopic trainer box.

REFERENCES

[1] Heizmann, O., Zidowitz, S., Bourquain, H., Potthast, S., Peitgen, H. O., Oertli, D., & Kettelhack, C. (2010). Assessment of intraoperative liver deformation during hepatic resection: prospective clinical study. *World journal of surgery*,*34*(8), 1887-1893.

[2] Clements, L. W., Chapman, W. C., Dawant, B. M., Galloway Jr, R. L., & Miga, M. I. (2008). Robust surface registration using salient anatomical features for image-guided liver surgery: Algorithm and validation. *Medical Physics*, *35*, 2528.

[3] Dumpuri, P., Clements, L. W., Dawant, B. M., & Miga, M. I. (2010). Model-updated image-guided liver surgery: preliminary results using surface characterization. *Progress in biophysics and molecular biology*, *103*(2), 197-207.

[4] Rucker, D. C., Wu, Y., Ondrake, J. E., Pheiffer, T. S., Simpson, A. L., & Miga, M. I. (2013, March). Nonrigid liver registration for image-guided surgery using partial surface data: a novel iterative approach. In *SPIE Medical Imaging* (pp. 86710B-86710B). International Society for Optics and Photonics.

[5] Viganò, L., Ferrero, A., Amisano, M., Russolillo, N., & Capussotti, L. (2013). Comparison of laparoscopic and open intraoperative ultrasonography for staging liver tumours. *British Journal of Surgery*, 535-542.

[6] Lorensen, W. E., & Cline, H. E. (1987, August). Marching cubes: A high resolution 3D surface construction algorithm. In *ACM Siggraph Computer Graphics* (Vol. 21, No. 4, pp. 163-169). ACM.

[7] Sullivan, J. M., Charron, G., & Paulsen, K. D. (1997). A three-dimensional mesh generator for arbitrary multiple material domains. Finite Elements in Analysis and Design, 25(3), 219-241.

[8] Simpson, A., Burgner, J., Glisson, C., Herrell, S., Ma, B., Pheiffer, T., ... & Miga, M. (2013). Comparison Study of Intraoperative Surface Acquisition Methods for Surgical Navigation. In *IEEE Transactions on Biomedical Engineering*(Vol 60 Issue 4).

[9] Conversano, F., Franchini, R., Demitri, C., Massoptier, L., Montagna, F., Maffezzoli, A., ... & Casciaro, S. (2011). Hepatic vessel segmentation for 3D planning of liver surgery: experimental evaluation of a new fully automatic algorithm. *Academic Radiology*, *18*(4), 461-470.

[10] Fong, Y., Jarnagin, W., Conlon, K. C., DeMatteo, R., Dougherty, E., & Blumgart, L. H. (2000). Hand-assisted laparoscopic liver resection: lessons from an initial experience. *Archives of Surgery*, *135*(7), 854.

[11] Burgner, J., Simpson, A. L., Fitzpatrick, J. M., Lathrop, R. A., Herrell, S. D., Miga, M. I., & Webster, R. J. (2012). A study on the theoretical and practical accuracy of conoscopic holography-based surface measurements: toward image registration in minimally invasive surgery. *The International Journal of Medical Robotics and Computer Assisted Surgery*.